Electrochemical Performance of Carbon/MnO2 Nanocomposites Prepared via Molecular Bridging as Supercapacitor Electrode Materials

Claudia Ramirez-Castro, Olivier Crosnier, Laurence Athouël, Richard Retoux, D. Belanger, Thierry Brousse

OPEN ACCESS

Electrochemical Performance of Carbon/MnO_2 Nanocomposites Prepared via Molecular Bridging as Supercapacitor Electrode Materials

To cite this article: C. Ramirez-Castro *et al* 2015 *J. Electrochem. Soc.* **162** A5179

JES Focus Issue on Electrochemical Capacitors: Fundamentals to Applications

Electrochemical Performance of Carbon/MnO_2 Nanocomposites Prepared via Molecular Bridging as Supercapacitor Electrode Materials

C. Ramirez-Castro,[a,b] O. Crosnier,[a,b,z] L. Athouël,[a,b] R. Retoux,[c] D. Bélanger,[d,*] and T. Brousse[a,b,*]

[a]*Institut des Matériaux Jean Rouxel (IMN), Université de Nantes, CNRS, 44322 Nantes Cedex 3, France*
[b]*Réseau sur le Stockage Electrochimique de l'Energie (RS2E), FR CNRS 3459, France*
[c]*Laboratoire CRISMAT UMR CNRS 6508, ENSICAEN, 14050 Caen Cedex, France*
[d]*UQÀM, Département de Chimie, Montréal, Québec H3C 3P8, Canada*

The chemical binding of amorphous manganese oxide and carbon particles was achieved with the diazonium chemistry. The synthesis was performed in two steps, with a first step consisting in the surface functionnalization of carbon particles with aminophenyl groups and the subsequent attachment of amorphous manganese oxide particles through generated phenyl groups. The bond between carbon and MnO_2 particles is believed to occur between the carbon from the phenyl groups attached to carbon particles, and the oxygen atoms from the manganese oxide lattice. The capacitance of the carbon/MnO_2 grafted nanocomposite electrode is doubled compared to a simple mixture of its two components. The capacitance of the nanocomposite electrode is also retained for faster cycling rates, thus highlighting the role of intimate coupling of carbon and MnO_2.
 [DOI: 10.1149/2.0221505jes] All rights reserved.

Manuscript submitted December 15, 2014; revised manuscript received January 23, 2015. Published February 26, 2015. *This paper is part of the JES Focus Issue on Electrochemical Capacitors: Fundamentals to Applications.*

The constant increment in the study and development of energy storage devices such as electrochemical capacitors (ECs) is related to an ever-growing demand of energy of the society. Electrochemical capacitors can be classified by their energy storage mechanisms in two main systems: 1) electrical double layer capacitance which arises from the charge separation at the electrode/electrolyte interface[1] and 2) pseudocapacitive charge storage phenomena where fast and reversible reactions take place.[2] At this time, carbon is the commonly used electrode material for electrical double layer capacitor (EDLC)[3] while transition metal oxides and some conductive metal nitrides have demonstrated good performance as pseudocapacitive electrodes.[4]

In terms of pseudocapacitive materials, manganese oxide (MnO_2) has proved to be one of the most promising materials due to its high energy density, low cost, environmental friendliness and natural abundance.[5] The initial studies describing the use of MnO_2 as an electrode material for ECs were performed by Lee and Goodenough.[6] They reported that amorphous or poorly crystallized MnO_2 powders incorporated into composite electrodes exhibited a capacitor-like electrochemical response in neutral KCl electrolyte, and delivered a specific capacitance of 200 F/g for "bulk" electrodes. Since this initial report, the interest in MnO_2 for ECs applications has grown steadily.

Despite its electrochemical performance, the use of MnO_2 is still limited to moderate power applications due to its poor intrinsic electrical conductivity (10^{-5} to 10^{-6} $S.cm^{-1}$).[7] Up to now, one of the most viable approaches to circumvent this major drawback is the use of a conductive additive such as carbon for improving the percolation through the electrode. For example, carbon black has been used just in a simple mixture with manganese oxide.[8,9] Other strategies consist in decorating different kinds of carbon particles with thin layers of MnO_2, generally obtained from chemical reduction of potassium permanganate or by more sophisticated deposition techniques such as chemical vapor deposition. Many carbon substrates have been investigated: standard carbon black,[10,11] activated carbon,[12] carbon nanofibers,[12] carbon nanotubes,[10,12–19] graphene,[10,20–22] microfibrous carbon paper[23] or microporous carbons.[24,25] Carbon coated MnO_2[26] or carbon/MnO_2 core-shell nanoparticles[27] have also been synthesized. Full device using two symmetrical carbon/MnO_2 nanocomposite electrodes have also been demonstrated.[28] From all these studies it is clear that an intimate mixture of the carbon additive and manganese dioxide leads to improved power capability, but there is no clear trend to tell which carbon additive leads to the best electrode. However, carbon black is already widely used in ECs technology and thus it should be desirable to focus on this type of carbon when designing MnO_2 based electrode.

In this study, we designed a new approach for the preparation of carbon/metal oxide composite electrodes based on the formation of a covalent bond between the conductive additive (carbon black) and the active material (manganese dioxide) by the use of diazonium chemistry.[29] Diazonium chemistry is a technique that consists in the reduction of a diazonium cation to generate an aryl radical that further reacts with a surface (metal, carbon, polymers or oxides) in order to form a covalent bond.[30] The versatility of this method allows the attachment of a large range of substituent aryl groups to many surfaces in order to change their surface properties or to immobilize specific chemical functionalities for different applications.[31]

Up to now, only few groups have reported the use of diazonium chemistry for bridging two materials through a phenyl group.[30] Since 2009 our group reported the bridging of carbon nanotubes (or graphite) and silicon nanoparticles for use in lithium-ion batteries.[32,33] The results show a better dispersion of both electrode components, drastically decreasing the electrode decrepitation upon cycling and also enhancing the electronic pathway through the electrode. The novelty of this scientific approach compared to existing literature on silicon/carbon nanocomposite was emphasized in different papers.[34–36] These results encourage the use of this diazonium chemistry for the improvement of electrode materials in other energy storage devices. The covalent attachment of electroactive molecules such as quinone for example, on the surface of activated carbon has shown drastic improvement of charge storage.[37–45] Very recently, Downard and coworkers demonstrated the possibility to covalently bind aryl group to MnO_2 nanorods from diazonium-based grafting,[46] assuming that such strategy can be used to improve electrochemical behavior of manganese dioxide based electrodes.

In this work, the chemical bridging between MnO_2 and carbon particles by diazonium chemistry is presented. The intimate contact between the two materials through a covalent bond can improve the

*Electrochemical Society Active Member.
[z]E-mail: Olivier.Crosnier@univ-nantes.fr

homogeneity between the carbon and MnO_2 particles as well as the electron transfer between them.

Experimental

Preparation of amorphous manganese oxides.— The so called "amorphous manganese oxide" (noted as MnO_2am in this study) was prepared by a standard coprecipitation technique.[6] Briefly, $KMnO_4$ (99% purity) was firstly dissolved in deionized water to reach a concentration of 0.05 M. While stirring the solution, a 0.05 M $MnSO_4$ solution was added dropwise. The $KMnO_4$ solution was kept in an ultrasonic bath during $MnSO_4$ addition. The $KMnO_4$:$MnSO_4$ molar ratio was 2:3. A dark brown precipitate was immediately obtained. The solution was then centrifuged at 9000 rpm and the precipitate was dried at 80°C for 2 h under primary vacuum. Finally, the powder was annealed in air at 200°C for 12 h. Five grams of powder were synthesized per batch.

Carbon modification.— In the first step, aminophenyl groups were grafted onto carbon particles by a previously reported synthesis method[47] where 1 g of carbon black (PUREBLACK) was dispersed in 100 mL of deionized water. Then, 1 equivalent of p-phenylenediamine (Sigma Aldrich) and 1 equivalent of sodium nitrite (98%, Alfa Aesar) were added. The solution was stirred until complete dissolution of the reactants and subsequently 10 mL of concentrated hydrochloric acid (12 M HCl) was added dropwise. The mixture was stirred overnight at room temperature and subsequently vacuum filtered. The modified carbon was washed several times with deionized water, methanol, dimethylformamide and acetone. Finally the powder was dried overnight at 60°C under vacuum. The resulting powder is made of carbon particles functionalized with aminophenyl groups since only one amine group was diazotized for further covalent bonding with carbon (Scheme 1, step 1).

Bridging amorphous manganese oxide and carbon through a phenyl group.— In the second step, 0.5 g of modified carbon and 0.5 g of manganese oxide were dispersed in 100 mL of acetronitrile and 3 eq. of tert-butylnitrite (tech. 90%, Alfa Aesar) were added. The mixture was stirred for 4 hours, vacuum filtered and washed with acetonitrile. The final powder was dried overnight at 60°C under vacuum. During this second step, the second amine group is diazotized and bridging of functionalized carbon with amorphous MnO_2 particles is expected (Scheme 1, step 2).

Characterization methods.— Scanning Electron Microscopy (SEM, MERLIN FE-SEM from ZEISS), Transmission Electron Microscopy (TEM, STEM) and X-ray Photoelectron Spectroscopy (XPS), were performed to fully characterize both bridged MnO_2am and carbon.

For SEM observations, the samples were sonicated in ethanol for 30 s and a few drops of the dispersed powder were then deposited onto the sampler holder and dried in an oven at 60°C for 1 hour before observation.

The TEM study was performed at room temperature using a 200 kV JEOL 2010 FEGSTEM transmission electron microscope fitted with a double tilt sample holder (tilt ± 42°). Samples were prepared by dispersing the different powders in ethanol by ultrasonic treatment; a few droplets of the suspensions were then deposited on a holey carbon film, supported by a copper grid. The chemical composition of the observed nanocomposites was determined by EDS mapping using the STEM (Scanning Transmission Electron Microscopy) option of the TEM using an EDAX EDS (Energy Dispersive Spectrometer).

The XPS analyses were performed by a Kratos Axis Nova using the Al Kα monochromatic beam (eV) with an input power of 144 W. The sample powders were dispersed onto adherent carbon film. The data were collected at room temperature and typically the operating pressure in the analysis chamber was kept below 10^{-9} Torr. XPS survey spectra were recorded with a pass energy of 120 meV, and the core level spectra were recorded with a pass energy of 50 meV. All spectra were corrected according to C 1s at 284.5 eV (graphite-like carbon).

Electrode preparation.— The electrodes were prepared by mixing the prepared material with PTFE in a 90/10 weight ratio with ethanol while heating at 60°C. Unlike many other studies, a carbon additive was not further added to the composition of the electrode since it is already present in the composite electrode. For all the samples the carbon to MnO_2 weight ratio was 50%. When all the ethanol was evaporated the mixture results in a rubber-like paste that was further cold rolled as a film (150 μm thick) on a flat glass surface. The resulting film was dried during 1 hour at 60°C. Electrodes with 12 mm diameter and a mass loading of ~10 mg.cm^{-2} were then cut and pressed between two stainless steel grids (ASI 316) at 9 ton.cm^{-2} for 2 minutes. The stainless steel grid was used as the current collector. Its double layer capacitance is negligible compared to that of the samples (less than 1%).

Electrochemical measurements.— The cyclic voltammetry (CV) experiments were carried out on a VMP3 multi-potentiostat (Bio-Logic) with EC-Lab as the software. A beaker-type cell containing a 5 M $LiNO_3$ electrolyte solution was used for all measurements. An Ag/AgCl (saturated NaCl) assembly and a platinum wire were used as the reference and counter electrodes, respectively. The CV experiments were performed between 0 and 0.9 V versus Ag/AgCl at different scan rates.

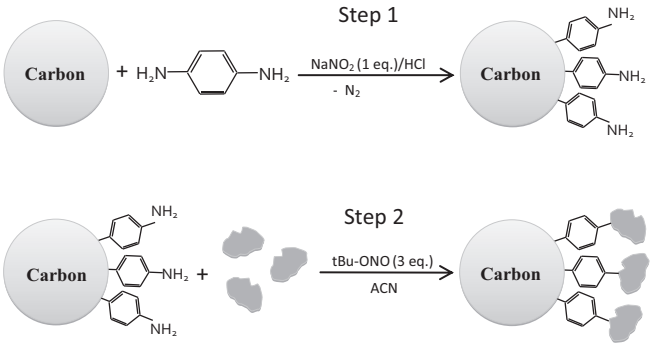

Scheme 1. Schematic reaction pathway for grafting carbon particles to MnO_2 grains. Step 1 corresponds to the first diazotation of the first amine group and the concomitant reduction of the diazonium cation; step 2 presents the diazotation of the remaining amine group and the concomitant reduction of the diazonium cation in order to bond both particles.

Results and Discussion

In order to compare the morphological, chemical and electrochemical properties of the bridged MnO_2am and carbon, a second sample, which consists of the simple mixture of MnO_2am and carbon particles was prepared. The first and second samples are referred to as MnO_2am-φ-C and MnO_2am+C throughout the manuscript, respectively. The amount of MnO_2 in each electrode is exactly the same (45% of the total weight of the composite electrode, i.e. ≈4.5 mg.cm^{-2}).

Figure 1 displays TEM images of 1.1) unmodified and 1.2) modified carbon (step 1 of synthesis) as well as 1.3) MnO_2am + non-grafted carbon and 1.4) MnO_2am-φ-C (step 2). Unmodified carbon (Fig. 1.1) presents a carbon multilayer typical aspect composed of stacked parallel layers of graphitic sheets with well-defined edges and a core constituted of an amorphous structure.

Figure 1.2 shows a TEM picture of the grafted carbon. The amorphous contrast typical of the grafted layer surrounding all the carbon grains is observed on the carbon multilayer grains as expected from step 1 of the reaction scheme (Scheme 1). On the enlargement presented in figure 1.2b, especially at the surface of the graphitic

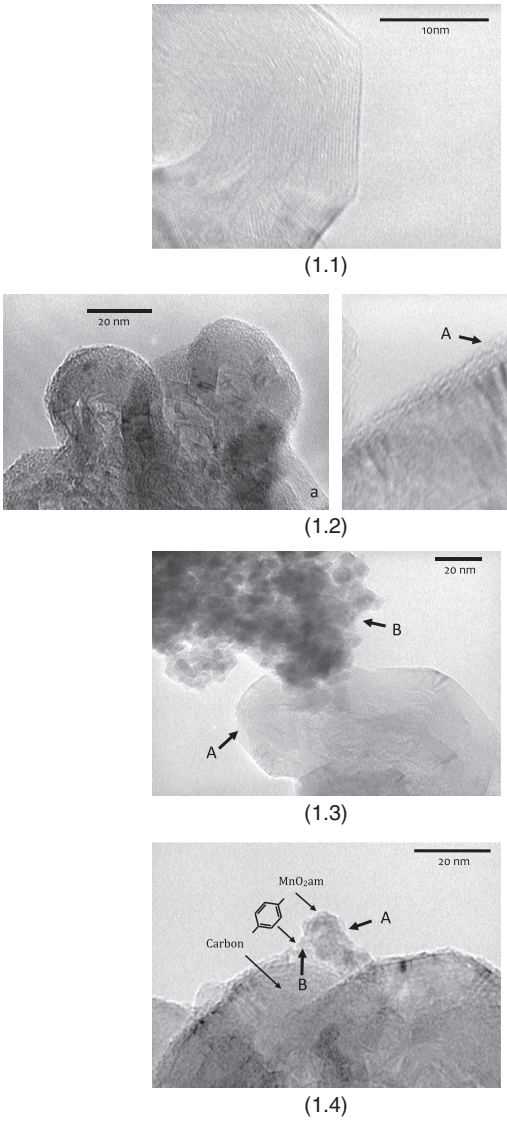

Figure 1. TEM images of 1.1) unmodified carbon black particle where the typical morphology of the grains and the carbon multilayer typical aspect of these grains composed of stacked parallel layers of graphitic sheets is clearly evidenced 1.2) modified carbon (step 1 of synthesis), arrow A label points (the amorphous characteristic contrasts of the organic layer surrounding the grains due to grafting on the surface of carbon black particles, 1.3) simple mixture of MnO_2am and carbon (arrow A is pointing at unmodified carbon black, and arrow B is showing amorphous MnO_2, namely MnO_2am) and 1.4) MnO_2 grafted to carbon particles (MnO_2am-φ-C, step 2 of synthesis); arrow A is pointing at a MnO_2am particle, arrow B is showing an organic layer linking a MnO_2am grain and a carbon black particle; a schematic picture of the link between carbon black and MnO_2am via molecular bridging is depicted for clarity purpose).

sheets, a blurred layer (pointed by a black arrow) corresponding to aminophenyl groups grafted onto carbon surface is clearly evidenced. It has to be noted that here, the grafted carbon images and contrasts are also blurred by the fact that the grafted layer is grafted all over the carbon and the observed contrasts are the result of the superposition of the multilayer carbon image with the typical amorphous contrasts of the grafted layer. The grafted layer thickness is about 24 Å, considering that one aminophenyl moiety size is 7.6 Å, then, an average of 3 layers of aminophenyl groups are chemically linked to the carbon surface. For the spontaneous functionalization of carbon black, Toupin and Bélanger[48] proposed that after the growth of the monolayer, multilayers can be formed by the attack of the aminophenyl radicals on the already grafted phenyl rings.

For the image corresponding to MnO_2am + non-grafted carbon mixture (fig 1.3), the coexistence between carbon particles at the bottom, and MnO_2am on the top, is observed. No chemical bond is established between them. The MnO_2am is evidenced (black arrow) while the carbon multilayer appears with sharp contrasts typical of those observed on the unmodified carbon particles presented in figure 1.1.

Finally, for MnO_2am-φ-C (fig 1.4), the A black arrow points an isolated MnO_2am grain (confirmed by EDS) grafted on the modified carbon. As shown in figure 1.2, a grafted multilayer is observed in the carbon grains. This grafted layer is also clearly evidenced (B part pointed by a black arrow) at the neck between the carbon particles and the MnO_2am grains as it forms a meniscus between the carbon-organic layer and the MnO_2am, which evidences the chemical bridging of these three species.

As already mentioned, the chemical identification of these MnO_2am particles has been confirmed by point EDS analyses. In an attempt to confirm the nature of the particles grafted at the carbon surface (MnO_2am-φ-C sample), a chemical mapping at lower magnification was carried out by EDS in the STEM mode. This STEM mapping is presented in Figure 2. Figure 2a shows a TEM image of groups of oxide particles (black particles pointed by arrows and surrounded by a white circle) while Figures 2b, 2c, 2d and 2e present the low resolution bright field image, the C k, O k, Mn k EDS mapping, respectively. In red (Fig. 2c), the carbon particles in the nanocomposite material as well as the organic layer at carbon surface are shown. In green (Fig. 2d) and blue (Fig. 2e) the O and Mn EDS signatures allows to clearly identify MnO_2am particles distribution in the carbon matrix. These analyses confirm that the particles bridged on the multi-layered carbon through phenyl groups are manganese oxide nanoparticles. Thus, both TEM observations and micro-EDS analyses support the reaction mechanism proposed in step 2 (Scheme 1).

Electron Diffraction patterns performed on the nanoparticles confirmed the amorphous character of these MnO_2 particles; in the insert of Figure 2a is presented the electron diffraction pattern recorded on the MnO_2 particles surrounded by the white circle.

Once the chemical attachment between MnO_2am and carbon particles was confirmed, XPS analysis was performed in order to get some insight on the possible nature of the chemical bond between them.

Figure 3 shows the Mn 3s and Mn 2p core level spectra for MnO_2am-φ-C and MnO_2am + C. The spectra do not show any significant difference before and after bridging which confirms that manganese atoms are not directly involved in the bridging process. The O 1s and C 1s core level spectra of MnO_2am-φ-C and MnO_2am + C

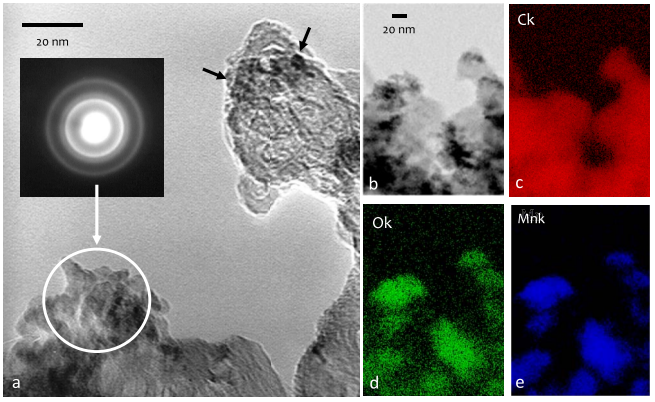

Figure 2. STEM mapping of (2a) groups of oxide particles (black particles pointed by arrows and surrounded by a white circle); bright field image (2b) and the Ck (2c), Ok (2d), Mnk (2e) mapping. The insert in Fig. 2a is the electron diffraction picture related to the oxide particles.

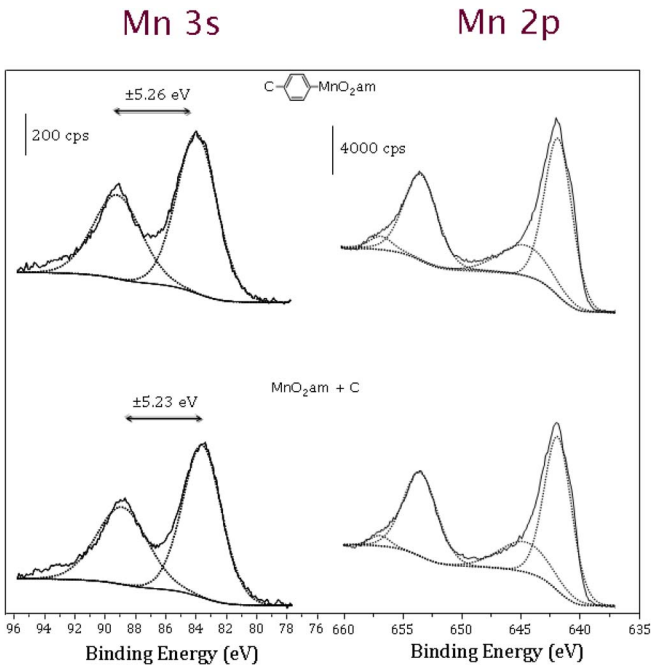

Figure 3. XPS Mn 3s and Mn 2p core level spectra for MnO_2am-φ-C and MnO_2am + C.

depicted in Figure 4 show that unlike the Mn 3s and Mn 2p spectra, the O 1s and C 1s core level spectra show noticeable differences before and after bridging. Both samples (pristine and grafted) show the expected O 1s peaks for Mn–O–Mn and Mn at binding energy of 529.5 and 531.5 eV, respectively (Fig. 4). Water traces can be detected for the pristine MnO_2am + C sample at 532.5 eV. However, for MnO_2am-φ-C, the O 1s signal corresponding to 531.5 eV increased and also, the new contribution observed at 534.0 eV can be attributed to oxygen atom of metal–O–C bonds.[29,49–51]

The C 1s spectra of both samples show a more important relative contribution of the peaks at 284.7 and 286.4 eV with respect to the

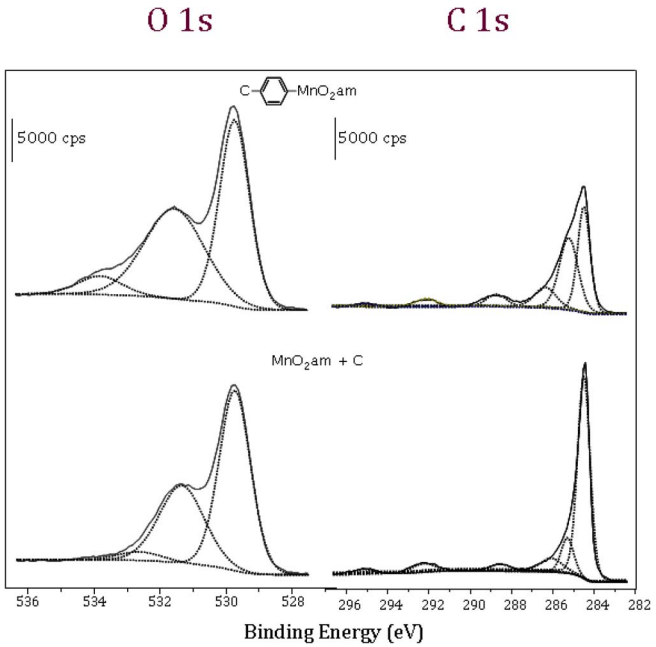

Figure 4. XPS O 1s and C 1s core level spectra of MnO_2am-φ-C and MnO_2am + C.

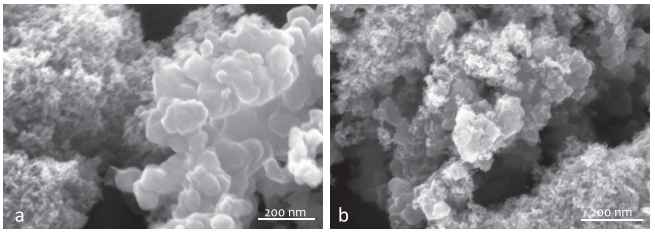

Figure 5. SEM images of the simple mixture MnO_2am + C (a) and the bridged sample MnO_2am-φ-C (b).

peak at 284.5 eV for MnO_2am-φ-C. The C 1s contribution near to 284.7 eV is related to benzene groups and its increase is in good agreement with the phenyl groups, which bond MnO_2am and carbon particles. According to literature data, a contribution related to C-O bond is present at 534.5 eV for O 1s and 286.0 eV for C 1s. Since the main changes in the XPS spectra of MnO_2am-φ-C occur at the same binding energy, the hypothesis that the bridging between MnO_2am and carbon occurs *via C-O* bond to form Mn-O-C bridges can be considered. However, the possible involvement of Mn-C bonds cannot be ruled out.[29]

More characterizations are required to establish the nature of the bond as well as a bridging pathway mechanism. The evidence found up to now implies that chemical bonds between the two powders are occurring through phenyl groups.

SEM images (Figure 5) of the simple mixture and the bridged sample were obtained in order to observe if the grafting process influenced the particle size distribution. For MnO_2am + C (a), on the left side of the image, the amorphous manganese oxide particles are built of a network of MnO_2am and pores, with a particle size less than 20 nm. On the right side of Figure 5a, the carbon particles consist of spherical carbon nanoparticles with a mean diameter of 50 nm. Both MnO_2am particles and carbon particles are agglomerated, thus preventing the intimate mixing of particles on the sample. On the other hand, the image corresponding to MnO_2am-φ-C (Fig. 5b) shows that the carbon particles are surrounded by manganese oxide particles. This observation evidences that the chemical coupling of both materials improves the particles distribution in the electrode.

Electrochemical experiments were performed in an attempt to highlight the influence of the chemical bond between MnO_2am and carbon, as well as the benefit of a better mixture of carbon and MnO_2am particles. Figure 6 shows the cyclic voltammograms of MnO_2am-φ-C and MnO_2am + C at 2 mV/s. For both materials, the

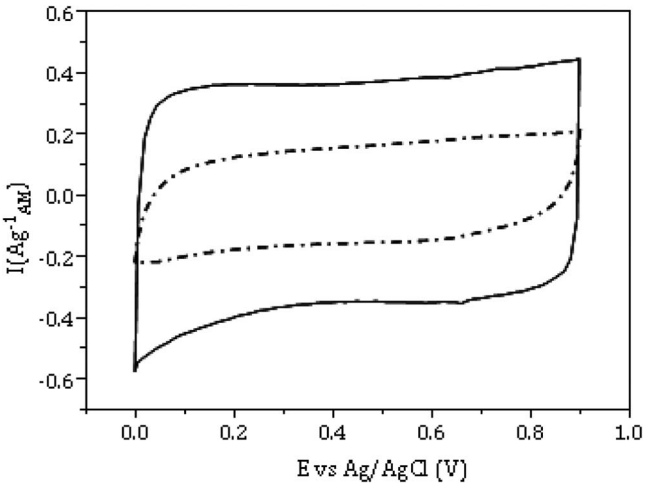

Figure 6. Cyclic voltammograms of MnO_2am-φ-C (full line) and MnO_2am + C (dashed line) electrodes in 5 M $LiNO_3$ aqueous electrolyte; at 2 $mV.s^{-1}$.

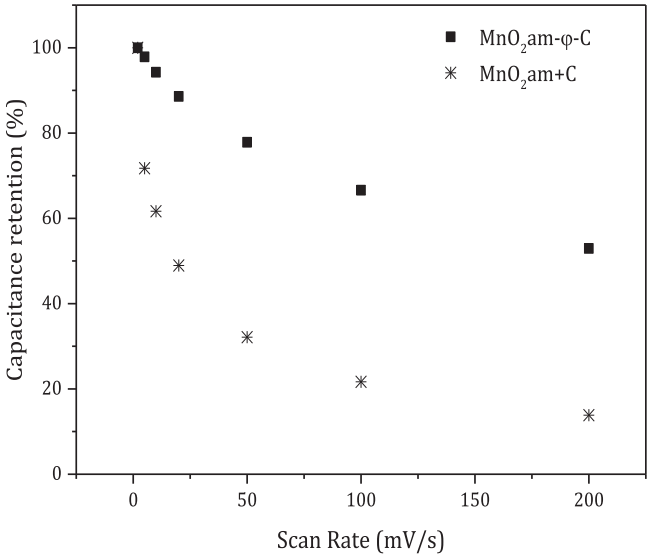

Figure 7. Relative capacitance versus scan rate for MnO_2am-φ-C and MnO_2am + C electrodes in 5 M $LiNO_3$ aqueous electrolyte.

shape of the CV is pseudo-rectangular, typical of the pseudocapacitive nature of MnO_2. This response has already been reported for amorphous manganese oxide-based electrodes in ECs.[52,53] The related capacitances (indicated per gram of MnO_2 in the electrode) are 185 and 55 F/g_{AM} (grams of active material) for MnO_2am-φ-C and MnO_2am + C electrodes, respectively. Even though a pseudo-rectangular shape is observed for the simple mixture of MnO_2am + C, the bridged MnO_2am-φ-C material shows an important increment of the current response as well as a more rectangular cyclic voltammogram which is related with a better electronic conductivity of the electrode. The intimate coupling between the particles is suspected to bring a lower charge transfer barrier, facilitating the electron transfer through the whole electrode. Also, the better dispersion between MnO_2am and carbon particles allows a greater amount of manganese oxide particles to participate in the charge storage process.

Figure 7 displays the scan rate dependence of the capacity retention of the two composite electrodes. MnO_2am-φ-C exhibits an important improvement in the capacity retention with respect to MnO_2am + C. At 200 mV/s, the bridged material still retains 53% of its maximum capacitance, while the simple mixture of MnO_2am and carbon only retains 14% of its initial value. This result is significant since the use of MnO_2-based electrodes for supercapacitors in practical applications will be governed by the rate capability of the electrodes.[52,54] Table I compares the power capability of different carbon/MnO_2 nanocomposite electrode. All the data published in the literature cannot be included in this table since the mass loading of the electrodes is often missing, thus preventing any meaningful comparison with the present work. Alternatively, the mass loading is so small (<1 $mg.cm^{-2}$) that the results cannot be extrapolated to larger electrodes.[55] Indeed, outstanding capacitance retention of 98% at 100 $mV.s^{-1}$ and impressive power capability have been reported for carbon nanotubes/MnO_2 nanocomposite but with only 0.5 $mg.cm^{-2}$.[14] One can see from Table I that when mass loadings larger than 2 $mg.cm^{-2}$ are used and with almost the same amount of MnO_2 in the electrode composition, the capacitance retention at 100 $mV.s^{-1}$ range from 31 to 69% without showing a clear trend for the role of the carbon substrate. Our grafting strategy leads to a capacitance retention of 62% which is on the upper range of all the electrode. In our case, only simple carbon black has been used instead of multiwalled carbon nanotubes or even graphene. Thus, the chemical coupling that we achieved using diazonium chemistry leads to interesting electrode performance that have to be further demonstrated in a real life cell.

Table I. Comparison of different carbon/MnO_2 nanocomposite electrodes and their capacitance retention.

%wt. MnO_2	Carbon type	Electrode loading ($mg.cm^{-2}$)	Capacitance retention*	Ref.
45%	MnO_2am-φ-C (Carbon black)	10	62%*	This work
45%	Carbon black	10	20%*	This work
69%	Carbon black	2	53%*	10
70%	Activated carbon	9.3	48%**	12
68%	Carbon coating	8.7	44%*	26
56%	Microporous carbon spheres	5	52%*	25
70%	Carbon nanofibers	9.3	31%**	12
43%	MWCNT†	10	12%*	15
70%	MWVNT	9.3	62%**	12
69%	MWCNT	2	58%*	10
-	MWCNT	1.8	50%*	16
25%	MWCNT	1.0	53%*	17
-	Graphene	0.3	33%*	20
69%	RGO‡	2	68%*	10
38%	Core-shell nanospheres	1.74	69%*	27

*Capacitance retention is defined as the ratio C(100 $mV.s^{-1}$)/C(2 $mV.s^{-1}$) or
**C(50 $mV.s^{-1}$)/C(2 $mV.s^{-1}$) when the value of capacitance at 100 $mV.s^{-1}$ was not available.
†Multiwall carbon nanotubes.
‡Reduced graphene oxide.

Conclusions

In the present study, the chemical coupling of amorphous manganese oxide and carbon particles through diazonium chemistry is presented. The synthesis was performed in two steps where carbon particles were grafted with aminophenyl groups and subsequently bonded to amorphous manganese oxide particles. The bond established between carbon and MnO_2am particles seems to occur between the carbon from the phenyl groups attached to carbon particles and the oxygen from the manganese oxide lattice. The improvement in the electrochemical response of the new material is related to a lower charge transfer barrier resulting in a better electronic pathway through the electrode. These results are encouraging for a further application of MnO_2-base electrodes in high power capability devices.

References

1. A. Burke, *J. Power Sources*, **91**, 37 (2000).
2. S. Pang, M. Anderson, and T. Chapman, *J. Electrochem. Soc.*, **147**, 444 (2000).
3. A. G. Pandolfo and A. F. Hollenkamp, *J. Power Sources*, **157**, 27 (2006).
4. B. Conway, Electrochemical Supercapacitors; Scientific Fundamentals and Technological Applications, Kluwer Academic/Plenum Publishers (1999).
5. Y. Hou, Y. Cheng, and J. Liu, *Nano Lett.*, **10**, 227 (2010).
6. H. Lee and J. Goodenough, *J. Solid State Chem.*, **144**, 220 (1999).
7. D. Belanger, T. Brousse, and J. Long, *Electrochem. Soc. Interface*, **17**, 49 (2008).
8. M. Toupin, T. Brousse, and D. Bélanger, *Chem Mater.*, **16**, 3184 (2004).
9. R. Reddy and R. Reddy, *J. Power Sources*, **124**, 330 (2003).
10. J. Zhang and X. S. Zhao, *Carbon*, **52**, 1 (2013).
11. A. Zolfaghari, H. R. Naderi, and H. R. Mortaheb, *J. Electroanal. Chem.*, **697**, 60 (2013).
12. Y. Zhang, Q.-Q. Yao, H.-L. Gao, L.-Z. Wang, X.-L. Jia, A.-Q. Zhang, Y.-H. Song, T.-C. Xia, and H-C. Dong, *Powder Technol.*, **262**, 150 (2014).
13. S. Lee, J. Kim, S. Chen, P. Hammond, and S. Y. Hao-Horn, *ACS Nano*, **4**, 3889 (2010).
14. K.-W. Nam, C.-W. Lee, X.-Q. Yang, B. Won Cho, W.-S. Yoon, and K.-B. Kim, *J. Power Sources*, **188**, 323 (2009).
15. X. Xie and L. Gao, *Carbon*, **45**, 2365 (2007).
16. Q. Li, J. M. Anderson, Y. Chen, and L. Zhai, *Electrochim. Acta*, **59**, 548 (2012).
17. J. Cai, M. He, Y. Gu, L. Kang, Z. Lei, Z. Yang, and Z.-H. Liu, *Colloids Surf. A*, **429**, 91 (2013).
18. T. Bordjiba and D. Bélanger, *Electrochim. Acta*, **55**, 3428 (2010).

19. Y. Wang, H. Liu, X. Sunb, and I. Zhitomirsky, *Scripta Mater.*, **61**, 1079 (2009).
20. G. Yu, L. Hu, M. Vosgueritchian, H. Wang, X. Xie, J. R. McDonough, X. Cui, Y. Cui, and Z. Bao, *Nano Lett.*, **11**, 2905 (2011).
21. Q. Tang, M. Sun, S. Yu, and G. Wang, *Electrochim. Acta*, **125**, 488 (2014).
22. S.-W. Lee, S.-M. Bak, C.-W. Lee, C. Jaye, D. A. Fischer, B.-K. Kim, X.-Q. Yang, K.-W. Nam, and K.-B. Kim, *J. Phys. Chem. C*, **118**, 2834 (2014).
23. T. Bordjiba and D. Bélanger, *J. Electrochem. Soc.*, **156**, A378 (2009).
24. Y. Lee, C. Fournier, J. Pascal, and F. Favier, *Microporous Mesoporous Mater.*, **110**, 167 (2008).
25. W. Wei, X. Huang,Y. Tao, K. Chen, and X. Tang, *Phys. Chem. Chem. Phys.*, **14**, 5966 (2012).
26. G. Wang, Y. Liu, G. Shao, L. Kong, and W. Gao, *ACS Sustainable Chem. Eng.*, **2**, 2191 (2014).
27. Y. Zhao, Y. Meng, and P. Jiang, *J. Power Sources*, **259**, 219 (2014).
28. S. Zhang, C. Peng, K. C. Ng, and G. Z. Chen, *Electrochim. Acta*, **55**, 7447 (2010).
29. C. Ramirez-Castro, *Ph. D. thesis, University of Nantes* (2012).
30. N. Griffete, F. Herbst, J. Pinson, S. Ammar, and C. Mangeney, *J. Am. Chem. Soc.*, **133**, 1646 (2011).
31. D. Bélanger and J. Pinson, *Chem. Soc. Rev.*, **40**, 3995 (2011).
32. C. Martin, O. Crosnier, R. Retoux, D. Bélanger, D. M. Schleich, and T. Brousse, *Adv. Funct. Mater.*, **21**, 3524 (2011).
33. C. Martin, M. Alias, F. Christien, O. Crosnier, D. Bélanger, and T. Brousse, *Adv. Mater.*, **21**, 4735 (2009).
34. S. Yang, G. Li, Q. Zhu, and Q. Pan, *J. Mater. Chem.*, **22**, 3420 (2012).
35. F. Alloin, L. Crepel, L. Cointeaux, J.-C. Leprêtre, F. Fusalba, and S. Martinet, *J. Electrochem. Soc.*, **160**, A3171 (2013).
36. G. Zeb, P. Gaskell, X. Tuan Le, X. Xiao, T. Szkopek, and M. Cerruti, *Langmuir*, **28**, 13042 (2012).
37. K. Kalinathan, D. P. DesRoches, X. Liu, and P. G. Pickup, *J. Power Sources*, **181**, 182 (2008).
38. Z. Algharaibeh, X. Liu, and P. G. Pickup, *J. Power Sources*, **187**, 640 (2009).
39. G. Pognon, T. Brousse, L. Demarconnay, and D. Bélanger, *J. Power Sources*, **196**, 4117 (2011).
40. Z. Algharaibeh and P. G. Pickup, *Electrochem. Commun.*, **13**, 147 (2011).
41. G. Pognon, T. Brousse, and D. Bélanger, *Carbon*, **49**, 1340 (2011).
42. L. Madec, A. Bouvrée, P. Blanchard, C. Cougnon, T. Brousse, B. Lestriez, D. Guyomard, and J. Gaubicher, *Energy Environ. Sci.*, **5**, 5379 (2012).
43. A. Le Comte, T. Brousse, and D. Bélanger, *Electrochim. Acta*, **137**, 447 (2014).
44. E. Lebègue, T. Brousse, J. Gaubicher, R. Retoux, and C. Cougnon, *J. Mater. Chem. A*, **2**, 8599 (2014).
45. A. Le Comte, D. Chhin, A. Gagnon, R. Retoux, T. Brousse, and D. Belanger, *J. Mater. Chem. A*, DOI: 10.1039/C4TA05536E (2015).
46. K. J. Bell, P. A. Brooksby, M. I. J. Polson, and A. J. Downard, *Chem. Commun.*, **50**, 13687 (2014).
47. M. Toupin and D. Bélanger, *J. Phys. Chem. C*, **111**, 5394 (2007).
48. M. Toupin and D. Bélanger, *Langmuir*, **24**, 1910 (2008).
49. B. L. Hurley and R. L. McCreery, *J. Electrochem. Soc.*, **151**, B252 (2004).
50. S. Akhter, X. L. Zhou, and J. M. White, *Appl. Surf. Sci.*, **37**, 201 (1989).
51. C. Dicke, M. Morstein, and G. Hahner, *Langmuir*, **18**, 336 (2002).
52. S. Ching, E. Welsh, S. Hughes, and A. Bahadoor, *Chem. Mater.*, **14**, 1292 (2002).
53. T. Brousse, M. Toupin, and D. Bélanger, *J. Electrochem. Soc.*, **151**, A614 (2004).
54. G. Lota, K. Lota, and E. Frackowiak, *Electrochem. Commun.*, **9**, 1828 (2007).
55. Y. Gogotsi and P. Simon, *Science*, **334**, 917 (2011).